Probing millicharge at BESIII via monophoton searches

Zuowei Liu[1,2,3,*] and Yu Zhang[4,1,3,†]

[1]*Department of Physics, Nanjing University, Nanjing 210093, China*
[2]*Center for High Energy Physics, Peking University, Beijing 100871, China*
[3]*CAS Center for Excellence in Particle Physics, Beijing 100049, China*
[4]*Institute of Physical Science and Information Technology, Anhui University, Hefei 230026, China*

We propose to search for millicharged particles at the BESIII detector which is operated at the Beijing Electron Positron Collider. We compute the monophoton signal events at the BESIII detector due to millicharged particle production, as well as due to standard model irreducible/reducible backgrounds. By utilizing all the data accumulated at the BESIII detector since 2011, we derive new leading upper limits on millicharge, $\varepsilon \lesssim (0.86\text{–}2.5) \times 10^{-3}$, for the mass range, $0.1 \text{ GeV} \lesssim m \lesssim 1 \text{ GeV}$. Furthermore, projections with more data to be collected at the BESIII detector are made. Our analysis significantly reduces the parameter region of millicharged dark matter to account for the anomalous 21 cm signal near redshift $z \simeq 17$ recently observed by the EDGES experiment.

I. INTRODUCTION

Electric charge quantization is an empirical fact. Charge quantization is also theoretically related to the magnetic monopole, because if any magnetic monopole exists in the Universe, it quantizes the electric charge [1]. However, so far, there is no clear experimental evidence to support the existence of the magnetic monopole. Thus we do not know yet what mechanism leads to electric charge quantization.

A number of experiments have been carried out to detect the noninteger charge of particles in the standard model (SM), and very stringent limits have been obtained. For example, the charge of hydrogen atom and neutron are measured to be smaller than $10^{-21}e$, where e is the magnitude of the electron charge [2–5]. There are also searches for new particles beyond the SM that carry electric charge, and very strong constraints on electrically charged new particles have been imposed from various laboratory experiments and astrophysical processes (see, e.g., [6–8] for the review on the constraints). The electrically charged particles beyond SM are referred as millicharged (or minicharged) particles, since usually only new particles with very small electric charge are allowed.

To parametrize the extremely weak coupling between a millicharged fermion and the SM photon, we employ the following interaction Lagrangian

$$\mathcal{L}_{\text{int}} = e\varepsilon A_\mu \bar{\chi}\gamma^\mu \chi, \tag{1}$$

where χ is the millicharged particle, A_μ is the SM photon, and ε is the millicharge (normalized to the magnitude of the electron charge). There are viable theoretical models in which millicharged particle can naturally occur. For example, millicharge particles may be present in models in which a kinetic mixing term is introduced between different $U(1)$ gauge fields [9,10]. Millicharged particles can also arise in Stueckelberg extensions of the SM in which mass terms generated by the Stueckelberg mechanism mix the SM $U(1)_Y$ gauge boson and new Abelian gauge bosons in the hidden sector beyond SM [11–13]. In this paper, we only consider the millicharged particle and the interaction given by Eq. (1); we decouple all other particles that appear in a specific model and do not consider any additional interaction between millicharged particles with SM.

Recently, an anomalous absorption signal near redshift $z \simeq 17$ in the cosmological 21 cm spectrum was observed by the EDGES experiment [14]. To explain such a signal, a number of papers have used millicharged dark matter (DM) particles to cool the hydrogen atom in the Universe. Our analysis in this paper has direct implications to the parameter space of millicharged particles that can explain the 21 cm anomaly [15–17].

In this paper, we propose to search for millicharged particles below GeV at the BESIII detector, which is operated at the Beijing Electron Positron Collider (BEPCII).

*zuoweiliu@nju.edu.cn
†dayu@nju.edu.cn

The existing laboratory constraints for MeV-GeV millicharged particles include bounds from the SLAC electron beam-dump experiment [18], bounds from the SLAC MilliQ searches [19], bounds from the E613 experiment [20], and bounds from MiniBooNE [21]. Recently, CMS collaboration [22] excludes particles with electric charge $2e/3$ ($e/3$) below 310 (140) GeV. There is also a proposed experiment at the LHC aiming to detect millicharged particles [23]. Here we use the monophoton signal to probe the MeV-GeV millicharged particles by analyzing the BESIII data of $\sim 15/\text{fb}$. The monophoton signature has been considered previously in DM searches at e^+e^- colliders [24–29]. Here we first carry out a detailed analysis at the BESIII detector by taking into account various backgrounds. We derive the BESIII sensitivity to the millicharge, and show that the BESIII detector can probe the parameter region that has not been constrained by previous experiments.

II. SIGNALS OF MILLICHARGED PARTICLES AT ELECTRON COLLIDERS

Millicharged particle can be produced at particle colliders via its coupling with the SM photon. However, if the millicharge is very small, the produced millicharged particle is often undetectable in practice, because only a feeble signature inside particle detectors could be produced. Thus one relies on final state particles produced in additional to the millicharged particle for the detection, which is analogous to most dark matter searches at particle colliders.

At the electron-positron collider, we use the monophoton signal to search for the millicharged particles, since the monophoton channel is the simplest channel to probe the millicharge at the electron collider. The Feynman diagram for the production process of the single photon in association with millicharged particles, $e^+e^- \to \chi\bar{\chi}\gamma$, is shown in Fig. 1, where χ stands for the millicharged particle.

The differential cross section for the $e^+e^- \to \chi\bar{\chi}\gamma$ process is given by

$$\frac{d\sigma}{dE_\gamma dz_\gamma} = \frac{8\alpha^3\epsilon^2(1 + 2m_\chi^2/s_\gamma)\beta_\chi}{3sE_\gamma(1 - z_\gamma^2)}\left[1 + \frac{E_\gamma^2}{s_\gamma}(1 + z_\gamma^2)\right], \quad (2)$$

where E_γ is the energy of the final state photon, $z_\gamma \equiv \cos\theta_\gamma$ with θ_γ being the relative angle between the final state photon and the beam direction of the initial state electron, s is the square of the center-of-mass energy, m_χ
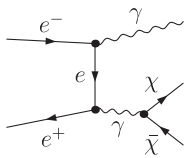

FIG. 1. Feynman diagram for the process $e^+e^- \to \chi\bar{\chi}\gamma$.
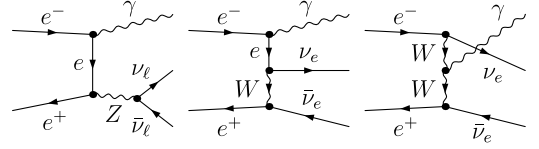

FIG. 2. Feynman diagrams for the process $e^+e^- \to \nu_\ell\bar{\nu}_\ell\gamma$, where $\nu_\ell = \nu_e, \nu_\mu, \nu_\tau$ [30,31].

is the mass of the millicharged particle, $s_\gamma = s - 2\sqrt{s}E_\gamma$, and $\beta_\chi = (1 - 4m_\chi^2/s_\gamma)^{1/2}$. Here we have integrated over all possible momenta for the two final state millicharged particles and neglected the electron mass.

III. THE IRREDUCIBLE BACKGROUND

The major irreducible SM background processes to the monophoton signal at the electron-positron collider are the $e^+e^- \to \nu_\ell\bar{\nu}_\ell\gamma$ processes, where $\nu_\ell = \nu_e, \nu_\mu, \nu_\tau$ are the three SM neutrinos. The corresponding Feynman diagrams are displayed in Fig. 2. The diagram with two W bosons is neglected for colliding energies at the GeV scale because it is much smaller than the other diagrams. The differential production cross section for the $e^+e^- \to \nu\bar{\nu}\gamma$ processes mediated by a single W/Z boson is given by [32,30]

$$\frac{d\sigma}{dE_\gamma dz_\gamma} = \frac{\alpha G_F^2 s_\gamma^2}{4\pi^2 sE_\gamma(1 - z_\gamma^2)}f(s_W)\left[1 + \frac{E_\gamma^2}{s_\gamma}(1 + z_\gamma^2)\right], \quad (3)$$

where G_F is the Fermi constant, $s_W \equiv \sin\theta_W$ with θ_W being the weak mixing angle, and $f(s_W) = 8s_W^4 - 4s_W^2/3 + 1$. Here we have integrated over the momenta of the final state neutrinos and summed all three neutrino flavors.

There are other irreducible SM backgrounds due to semi-invisible meson decays, e.g., $J/\psi \to \nu\bar{\nu}\gamma$. However, the branching ratio of these decay modes are typically very small, for instance, $\text{BR}(J/\psi \to \nu\bar{\nu}\gamma) = 0.7 \times 10^{-10}$ in SM [33]. Thus we exclude those irreducible backgrounds in meson decays in our analysis.

IV. REDUCIBLE BACKGROUNDS AT THE BESIII DETECTOR

Next we want to investigate the reducible backgrounds at the BESIII detector, which is located at the double-ring BEPCII with the beam energy ranging from 1.0 GeV to 2.3 GeV [34]. The reducible backgrounds are present due to the limited detection capability of the BESIII subdetectors. The main drift chamber (MDC) covers the polar angle $|\cos\theta| < 0.93$ [34]. The electromagnetic calorimeter (EMC) consists of the barrel with angle coverage $|\cos\theta| < 0.83$ and the endcap with angle coverage $0.85 < |\cos\theta| < 0.93$ [34]. The time-of-flight (TOF) subdetector consists of the barrel with angle coverage $|\cos\theta| < 0.83$ and the endcap with angle coverage $0.85 < |\cos\theta| < 0.95$ [34].
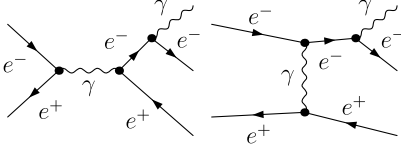
FIG. 3.   Feynman diagram for the process $e^+e^- \rightarrow e^+e^-\gamma$.

One of the most important reducible backgrounds arises from the radiative Bhabha scattering, $e^+e^- \rightarrow e^+e^-\gamma$, where neither of the two final state electrons is detected. There are eight diagrams in the radiative Bhabha scattering, two of which are shown in Fig. 3.

The reducible backgrounds also include the $e^+e^- \rightarrow \bar{f}f\gamma$ background where the final state f fermion ($f \neq e$) escapes detection, and the $e^+e^- \rightarrow \gamma\gamma\gamma$ process where only one of the three final state photons is detected. There are also reducible backgrounds from meson decays in which a final state photon is accompanied by several other particles going along beam directions. We consider all these reducible backgrounds in our analysis.

V. DETECTOR SIMULATION

We simulate signal events and different SM background events for various BESIII running energies, which are shown in Table II. For the signal process $e^+e^- \rightarrow \chi\bar{\chi}\gamma$ and the irreducible background $e^+e^- \rightarrow \nu\bar{\nu}\gamma$, we generated one million points from the analytic differential cross sections, Eqs. (2) and (3), in the $E_\gamma - z_\gamma$ plane using Monte-Carlo methods.

The simulations for the $e^+e^- \rightarrow e^+e^-\gamma$ background need extra care because the collinear singularities in the radiative Bhabha scattering, which arise in the t-channel photon processes in Fig. 3, dominate the total cross section [35–38]. We use FEYNARTS [39] and FORMCALC [40] packages to numerically evaluate the cross section for the process $e^+e^- \rightarrow e^+e^-\gamma$ where the final state $e^\pm$ has $|\cos\theta| > 0.95$, which is beyond the coverage of the TOF, as well as MDC and EMC. We found that MADGRAPH [41] cannot sample the phase space efficiently due to the collinear singularity. We carry out similar calculations for $e^+e^- \rightarrow \mu^+\mu^-\gamma$ and $e^+e^- \rightarrow \gamma\gamma\gamma$. We impose $E_\gamma > 1$ MeV [42] to remove the infrared divergence in $e^+e^- \rightarrow \gamma\gamma\gamma$. The reducible backgrounds from meson decays are simulated using EVTGEN [43,44].

The energy and position information of photon and electron are determined by the EMC. The energy resolution of the EMC at the BESIII detector is [34]

$$\sigma(E)/E = 2.3\%/\sqrt{E/\text{GeV}} \oplus 1\%. \qquad (4)$$

The angular resolution also depends on the energy of the particle; we provided the following fitted function which gives a nice approximation to the angular resolution [45]

$$\sigma(\theta) = (0.024/\sqrt{E/\text{GeV}} - 0.002)(\text{rad}). \qquad (5)$$

To simulate the detector effects on the final state particles, we smear the energy and the polar angle for the final state electron and photon using Gaussian distributions which take into account the resolution functions, Eqs. (4) and (5).

VI. DETECTOR CUTS

The energy measurement for electrons or photons in the EMC at the BESIII detector ranges from 20 MeV to 2 GeV. We follow the cuts used by the BESIII Collaboration [46]: (hereafter the basic cuts) photon candidates must satisfy $E > 25$ MeV in the barrel ($|\cos\theta| < 0.8$) or $E > 50$ MeV in the end-caps ($0.86 < |\cos\theta| < 0.92$).

However, after the basic cuts, the reducible background due to $e^+e^- \rightarrow e^+e^-\gamma$ is still very large, as shown in Fig. 4 where we display $E_\gamma - z_\gamma$ normalized distributions for both the monophoton events due to millicharged particle production process and the $e^+e^- \rightarrow e^+e^-\gamma$ process. To suppress the big reducible backgrounds, we further impose the following cuts (hereafter the advanced cuts) on top of the basic cuts:

$$E_\gamma/\text{GeV} > az_\gamma^2 + b, \qquad (6)$$

where a and b are free parameters to be fixed by maximizing the significance. The advanced cuts are motivated by the fact that the final photon in the central region ($|\cos\theta| \ll 1$) cannot have a sufficient large energy due to energy conservation in the $e^+e^- \rightarrow e^+e^-\gamma$ process with both final $e^\pm$ going along the beam directions.
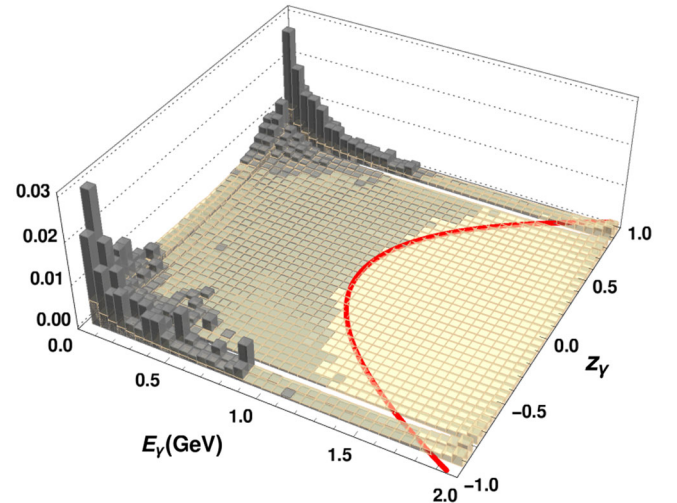

FIG. 4.   Photon $E_\gamma - z_\gamma$ normalized distributions in $e^+e^- \rightarrow \chi\bar{\chi}\gamma$ with $m_\chi = 0.1$ GeV (yellow) and in $e^+e^- \rightarrow e^+e^-\gamma$ (gray) at $\sqrt{s} = 4.18$ GeV. The red curve is $E_\gamma/\text{GeV} = 0.99z_\gamma^2 + 0.99$.

TABLE I. The cross sections (in unit of fb) of the signal and SM background processes (labeled by the final state) after each cut, and the corresponding significance $\mathcal{S} = S/\sqrt{S+B}$. The integrated luminosity is $\mathcal{L} = 1$ fb^{-1} and the running energy is $\sqrt{s} = 4.18$ GeV. We choose $m_\chi = 0.1$ GeV and $\varepsilon = 0.01$ for the millicharged particle. The advanced cut here is $E_\gamma/\text{GeV} > 0.99z_\gamma^2 + 0.99$.

Cuts	$\chi\bar{\chi}\gamma$	$\nu\bar{\nu}\gamma$	$e^+e^-\gamma$	$\mu^+\mu^-\gamma$	$\gamma\gamma\gamma$	$\mathcal{S}$
Basic	32.3	1.39	6.9×10^7	2.6×10^4	4.5×10^5	0.0038
Advanced	6.58	0.022	0	0	0	2.56

The $e^+e^- \to \mu^+\mu^-\gamma$ and $e^+e^- \to \gamma\gamma\gamma$ background processes exhibit similar distributions. As shown in Table I and in Fig. 4, the advanced cuts are very efficient in eliminating these reducible backgrounds.

We optimize the advanced cuts for each BESIII running energy by choosing the a and b values that maximize the significance for the case in which $m_\chi = 0.1$ GeV and $\varepsilon = 0.01$. Four SM backgrounds are considered in the optimization, including $e^+e^- \to \nu\bar{\nu}\gamma$, $e^+e^- \to e^+e^-\gamma$, $e^+e^- \to \gamma\gamma\gamma$, and the reducible background in meson decays. Table II shows the optimized a and b values for each running energy at BESIII. We have checked that under the optimized advanced cuts, the $e^+e^- \to \mu^+\mu^-\gamma$ process does not contribute any background event.

VII. METHODOLOGY OF COMBINING DATA

A large amount of data have been accumulated by the BESIII detector at various running energies since 2011 when the monophoton trigger was implemented [49]. A summary of the BESIII data is presented in Table II where the data are arranged by the center-of-mass energy $\sqrt{s}$. To probe the millicharge, we carry out a likelihood analysis to combine all the data collected at various running energies as shown in Table II. We first define a chi-square at each running energy, $\chi_i^2 = S_i/\sqrt{S_i + B_i}$, where S_i (B_i) is the number of signal (background) events at the running energy labeled by the index i. Here B_i includes the SM irreducible background, the SM reducible backgrounds, and other possible background events caused by instruments. We further build a likelihood function $\mathcal{L}_i$ for each running energy, $\mathcal{L}_i = \exp\left(-\chi_i^2/2\right)$. The total likelihood function $\mathcal{L}$ for combing all the running energies can be built via $\mathcal{L} = \Pi_i w_i \mathcal{L}_i$, where w_i is the weight for each running energy. The test-statistic (TS) is related to the total likelihood via $\text{TS} = -2\ln\mathcal{L}$. The 95% confidence level (C.L.) exclusion limit on the millicharge ε is obtained by demanding that the corresponding TS is larger by 2.71 than that in SM. In our analysis, we set $w_i = 1$ for all data points.

TABLE II. The center-of-mass energy and corresponding luminosities collected since 2011 at the BESIII detector, and the corresponding optimized a and b parameters for the advanced cuts. ε_{95} is the 95% C.L. upper limit on millicharge ε for the $m_\chi = 0.1$ GeV case. Data before 2017 are given by [47], and information about 2017 data is provided by [48]. The last row shows the limit combining all data between 2011 and 2017.

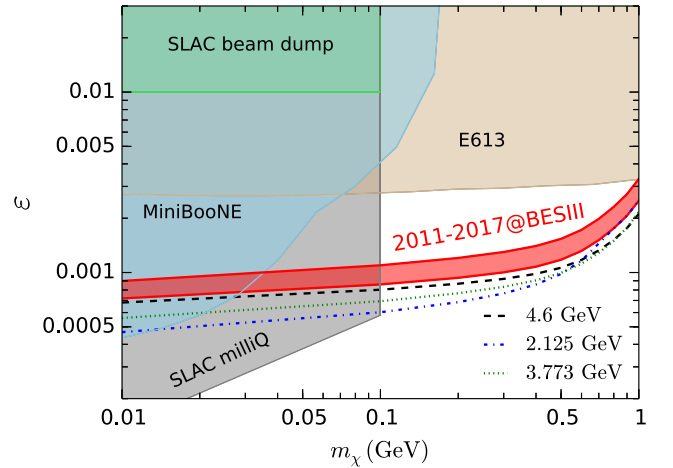| Year	$\sqrt{s}$ (GeV)	$\mathcal{L}$ (fb^{-1})	a	b	ε_{95}
2015	2.125	0.1	0.52	0.53	0.015
2012	3.097	0.32	0.68	1.12	0.015
2017	3.515	0.5	0.79	0.86	0.0095
2011	3.554	0.024	0.84	0.86	0.044
2012	3.686	0.51	0.95	1.21	0.013
2011	3.773	1.99	0.89	0.94	0.0051
2017	3.872	0.2	0.90	0.96	0.016
2011	4.009	0.5	0.92	0.98	0.011
2016	4.18	3.1	0.99	0.99	0.0060
2013	4.23	1.05	1.00	1.01	0.011
2013	4.26	0.83	1.01	1.02	0.013
2017	4.28	3.9	1.04	1.04	0.0063
2012	4.36	0.5	1.06	1.05	0.019
2014	4.42	1	1.02	1.08	0.014
2014	4.6	0.5	1.04	1.14	0.024
11–17	$\cdots$	15.024	$\cdots$	$\cdots$	8.6×10^{-4}

FIG. 5. The expected 95% C.L. exclusion limits on millicharged particles corresponding to the BESIII data collected during 2011-2017. The upper (lower) edge of the red band corresponds to the assumption where five (zero) more events appear in the BESIII data which are caused by instruments. The black-dashed (blue-dotdashed, green-dotted) line is the projected limit by assuming an additional 10 (10, 15) fb^{-1} data in future BESIII runs with $\sqrt{s} = 4.6(2.125, 3.773)$ GeV. Existing bounds are shown as shaded regions: bounds from the SLAC electron beam-dump experiment [18], bounds from the SLAC MilliQ searches [19], bounds from E613 [20], and bounds from Mini-BooNE [21].

VIII. RESULTS

Figure 5 shows the combined 95% C.L. exclusion upper limits on millicharge ε for various masses, by using the data presented in Table II. Here we further consider other possible background events that are caused by instruments. As shown in Fig. 5, the current BESIII data can probe millicharge down to $\varepsilon \lesssim 0.86(2.5) \times 10^{-3}$ for the $m_\chi = 0.1(1)$ GeV case. Figure 5 further shows preexisting experimental constraints in the $0.01 \text{ GeV} \lesssim m_\chi \lesssim 1 \text{ GeV}$ mass range, which include bounds from the SLAC electron beam-dump experiment [18], bounds from the SLAC MilliQ searches [19], bounds from E613 [20], and bounds from MiniBooNE [21]. Thus, BESIII data can provide new leading upper limits to the millicharged particle in the mass range, $0.1 \text{ GeV} \lesssim m_\chi \lesssim 1 \text{ GeV}$. The new limits significantly reduce the parameter space in which one can use 1%-10% millicharged DM to explain the 21 cm anomaly [15–17].

We further make projections in the future BESIII runs. Three different projected limits are drawn on Fig. 5 with additional 10 fb^{-1} data at $\sqrt{s} = 2.125$ GeV, additional 10 fb^{-1} data at $\sqrt{s} = 4.6$ GeV, and additional 15 fb^{-1} data at $\sqrt{s} = 3.773$ GeV [50]. Realistic data takings with more running energies can be interpolated between these projected limit lines.

IX. SUMMARY

In this paper, we have proposed a search for millicharged particles via the monophoton signature at the BESIII detector at BEPCII. We found that by using the current BESIII data, one can provide new leading constraints on the millicharged particle in the mass range, $0.1 \text{ GeV} \lesssim m_\chi \lesssim 1 \text{ GeV}$. We also systematically analyzed the irreducible and reducible SM backgrounds for the monophoton signature that are essential for dark matter searches at the BESIII detector which was lacking in the literature to our knowledge.

[1] P. A. M. Dirac, Proc. R. Soc. A **133**, 60 (1931).

[2] M. Marinelli and G. Morpurgo, Phys. Lett. B **137**, 439 (1984).

[3] G. Bressi, G. Carugno, F. Della Valle, G. Galeazzi, G. Ruoso, and G. Sartori, Phys. Rev. A **83**, 052101 (2011).

[4] J. Baumann, J. Kalus, R. Gahler, and W. Mampe, Phys. Rev. D **37**, 3107 (1988).

[5] C. Siemensen, C. Dsing, P. Geltenbort, C. Giebel, T. Reich, and C. Plonka, Phys. Rev. D **97**, 052004 (2018).

[6] S. Davidson and M. E. Peskin, Phys. Rev. D **49**, 2114 (1994).

[7] S. Davidson, S. Hannestad, and G. Raffelt, J. High Energy Phys. 05 (2000) 003.

[8] J. Jaeckel and A. Ringwald, Annu. Rev. Nucl. Part. Sci. **60**, 405 (2010).

[9] B. Holdom, Phys. Lett. B **166**, 196 (1986).

[10] B. Holdom, Phys. Lett. B **178**, 65 (1986).

[11] B. Kors and P. Nath, Phys. Lett. B **586**, 366 (2004).

[12] K. Cheung and T. C. Yuan, J. High Energy Phys. 03 (2007) 120.

[13] D. Feldman, Z. Liu, and P. Nath, Phys. Rev. D **75**, 115001 (2007).

[14] J. D. Bowman, A. E. E. Rogers, R. A. Monsalve, T. J. Mozdzen, and N. Mahesh, Nature (London) **555**, 67 (2018).

[15] J. B. Muoz and A. Loeb, Nature (London) **557**, 684 (2018).

[16] A. Berlin, D. Hooper, G. Krnjaic, and S. D. McDermott, Phys. Rev. Lett. **121**, 011102 (2018).

[17] R. Barkana, N. J. Outmezguine, D. Redigolo, and T. Volansky, Phys. Rev. D **98**, 103005 (2018).

[18] S. Davidson, B. Campbell, and D. C. Bailey, Phys. Rev. D **43**, 2314 (1991).

[19] A. A. Prinz et al., Phys. Rev. Lett. **81**, 1175 (1998).

[20] D. E. Soper, M. Spannowsky, C. J. Wallace, and T. M. P. Tait, Phys. Rev. D **90**, 115005 (2014).

[21] G. Magill, R. Plestid, M. Pospelov, and Y. D. Tsai, arXiv:1806.03310.

[22] S. Chatrchyan et al. (CMS Collaboration), Phys. Rev. D **87**, 092008 (2013).

[23] A. Haas, C. S. Hill, E. Izaguirre, and I. Yavin, Phys. Lett. B **746**, 117 (2015).

[24] N. Borodatchenkova, D. Choudhury, and M. Drees, Phys. Rev. Lett. **96**, 141802 (2006).

[25] S. h. Zhu, Phys. Rev. D **75**, 115004 (2007).

[26] P. Fayet, Phys. Rev. D **75**, 115017 (2007).

[27] R. Essig, P. Schuster, and N. Toro, Phys. Rev. D **80**, 015003 (2009).

[28] Z. H. Yu, Q. S. Yan, and P. F. Yin, Phys. Rev. D **88**, 075015 (2013).

[29] R. Essig, J. Mardon, M. Papucci, T. Volansky, and Y. M. Zhong, J. High Energy Phys. 11 (2013) 167.

[30] K. J. F. Gaemers, R. Gastmans, and F. M. Renard, Phys. Rev. D **19,** 1605 (1979).

[31] T. Araki, S. Hoshino, T. Ota, J. Sato, and T. Shimomura, Phys. Rev. D **95,** 055006 (2017).

[32] E. Ma and J. Okada, Phys. Rev. Lett. **41,** 287 (1978); **41** 1759(E) (1978).

[33] D. N. Gao, Phys. Rev. D **90,** 077501 (2014).

[34] D. M. Asner *et al.*, Int. J. Mod. Phys. A **24,** 9 (2009).

[35] C. Mana and M. Martinez, Nucl. Phys. **B287,** 601 (1987).

[36] K. Tobimatsu and Y. Shimizu, Comput. Phys. Commun. **55,** 337 (1989).

[37] K. Tobimatsu and M. Igarashi, Comput. Phys. Commun. **136,** 105 (2001).

[38] S. Actis, P. Mastrolia, and G. Ossola, Phys. Lett. B **682,** 419 (2010).

[39] T. Hahn, Comput. Phys. Commun. **140,** 418 (2001).

[40] T. Hahn and M. Perez-Victoria, Comput. Phys. Commun. **118,** 153 (1999).

[41] J. Alwall, R. Frederix, S. Frixione, V. Hirschi, F. Maltoni, O. Mattelaer, H.-S. Shao, T. Stelzer, P. Torrielli, and M. Zaro, J. High Energy Phys. 07 (2014) 079.

[42] Reducing the soft photon cut from $E_\gamma > 1$ MeV to $E_\gamma > 0.01$ MeV does not alter the advanced cuts nor the monophoton events in the $e^+e^- \to \gamma\gamma\gamma$ process after the advanced cuts.

[43] D. J. Lange, Nucl. Instrum. Methods Phys. Res., Sect. A **462,** 152 (2001).

[44] R. G. Ping, Chin. Phys. C **32,** 599 (2008).

[45] V. Prasad, C. Liu, X. Ji, W. Li, H. Liu, and X. Lou, Springer Proc. Phys. **174,** 577 (2016).

[46] M. Ablikim *et al.* (BESIII Collaboration), Phys. Rev. D **96,** 112008 (2017).

[47] http://bes3.ihep.ac.cn/datasets/datasets.htm.

[48] Jianlei Zhang (private communication).

[49] Dayong Wang (private communication).

[50] Hai-Bo Li (private communication).